CrystEngComm

RSC Publishing

PAPER

Self-assembled $Mg_xZn_{1-x}O$ quantum dots ($0 \leqslant x \leqslant 1$) on different substrates using spray pyrolysis methodology

Sreekumar Rajappan Achary,[a] Said Agouram,[a] Juan F. Sánchez-Royo,[ab] Manuel Lopez-Ponce,[c] J. M. Ulloa,[c] E. Muñoz,[c] A. Hierro[c] and Vicente Muñoz-Sanjosé*[a]

By using the spray pyrolysis methodology in its classical configuration we have grown self-assembled $Mg_xZn_{1-x}O$ quantum dots (size $\sim$4–6 nm) in the overall range of compositions $0 \leqslant x \leqslant 1$ on c-sapphire, Si (100) and quartz substrates. Composition of the quantum dots was determined by means of transmission electron microscopy-energy dispersive X-ray analysis (TEM-EDAX) and X-ray photoelectron spectroscopy. Selected area electron diffraction reveals the growth of single phase hexagonal $Mg_xZn_{1-x}O$ quantum dots with composition $0 \leqslant x \leqslant 0.32$ by using a nominal concentration of Mg in the range 0 to 45%. Onset of Mg concentration about 50% (nominal) forces the hexagonal lattice to undergo a phase transition from hexagonal to a cubic structure which resulted in the growth of hexagonal and cubic phases of $Mg_xZn_{1-x}O$ in the intermediate range of Mg concentrations 50 to 85% ($0.39 \leqslant x \leqslant 0.77$), whereas higher nominal concentration of Mg $\geqslant$ 90% ($0.81 \leqslant x \leqslant 1$) leads to the growth of single phase cubic $Mg_xZn_{1-x}O$ quantum dots. High resolution transmission electron microscopy and fast Fourier transform confirm the results and show clearly distinguishable hexagonal and cubic crystal structures of the respective quantum dots. A difference of 0.24 eV was detected between the core levels (Zn 2p and Mg 1s) measured in quantum dots with hexagonal and cubic structures by X-ray photoemission. The shift of these core levels can be explained in the frame of the different coordination of cations in the hexagonal and cubic configurations. Finally, the optical absorption measurements performed on single phase hexagonal $Mg_xZn_{1-x}O$ QDs exhibited a clear shift in optical energy gap on increasing the Mg concentration from 0 to 40%, which is explained as an effect of substitution of Zn^{2+} by Mg^{2+} in the ZnO lattice.

Introduction

The development of nanotechnology, both at academic and industrial levels, has allowed an advance in the miniaturization of optoelectronic and electronic devices and it has allowed a significant step to the increase in data storage capacity.[1–3] In order to improve the existing technology, intense research is being carried out on nanostructured materials, namely on zero dimensional materials. Zero dimensional materials, known as quantum dots (QDs), in which the electronic motion is confined in all the three spacial dimensions, are of technological importance due to interesting enhanced excitonic radiative recombination and size-dependent tuning of spectral emissions towards short-wavelength region.[4] Quantum confinement effects modify the profile of density of states in quantum dots so that the transfer integral at the band-edge enhances much higher than in bulk or quantum wells, facilitating efficient stimulated emission and resulting in high efficient operation of devices at low threshold energy density.[5] Due to the technological importance, quantum dots of various materials InAs, GaAs, InP, CdS, ZnO are being widely studied. More in particular, ZnO has gained utmost attention among researchers due to its possible applications in short-wavelength lasers and LEDs.[5–9] One of the features of ZnO is its band gap potential tunability to a wide range from 3.37 to 6.7 eV *via* magnesium incorporation into ZnO lattice ($Mg_xZn_{1-x}O$).[10] Films of $Mg_xZn_{1-x}O$ exist in two different phases with hexagonal and cubic structures depending on the Mg concentration.[10,11] Maintaining hexagonal structure the optical band gap of $Mg_xZn_{1-x}O$ could be enhanced up to 4.3 eV,[11] whereas the cubic phase takes the advantage of extending the band gap to a value very close to 6.7 eV.[10] The

[a]*Departamento de Fisica Aplicada y Electromagnetismo, Universitat de Valencia, C/Dr. Moliner 50, Burjassot, Valencia 46100, Spain. E-mail: Vicente.Munoz@uv.es; Fax: + 34 963543146; Tel: +34 963544617*
[b]*Instituto de Ciencia de Materiales, Universitat de Valencia, C/Dr. Moliner 50, Burjassot, Valencia 46100, Spain*
[c]*Instituto de Sistemas Optoelectrónicos y Microtecnología, Dept. Ing. Electrónica, Univ. Politecnica Madrid, Madrid, Spain*

possibility of tuning the band gap in $Mg_xZn_{1-x}O$ to higher energies is encouraging for current technology of UV lasers and photo-detectors. Until now, major research works have been focused on $Mg_xZn_{1-x}O$ thin films,[12–14] and there are only few reports published on the growth of $Mg_xZn_{1-x}O$ QDs[15] or free nanoparticles/nanostructures.[16–20] In particular, Zeng et al.[15] obtained $Mg_xZn_{1-x}O$ QDs of size ~9 nm on Si (100) substrates using low pressure Metal Organic Chemical Vapour Deposition (MOCVD) technique. However the study was limited only up to 2.3 at% of Mg incorporation into the ZnO lattice. Table 1 summarizes the range of compositions, sizes and the different phases of $Mg_xZn_{1-x}O$ nanoparticles obtained by various researchers using different growth techniques.[21,22]

Recently our group showed the availability of the spray pyrolysis (SP) methodology for the growth of zero dimensional ZnO QDs on various substrates (c-Al_2O_3, quartz and glass).[23] By controlling the precursor concentration, growth temperature and growth time, a wide range of QD densities (~2 × 10^{10} to 3.5 × 10^{11} QDs cm^{-2}) and sizes (5 to 14 nm) were obtained. In the present work, by using the SP technique we focus on the growth of $Mg_xZn_{1-x}O$ quantum dots on c-sapphire and Si (100) substrates, which have different crystal structures and are present in current technology. We have carried out a systematic study of the incorporation of Mg into the ZnO lattice, and vice versa, Zn on the MgO lattice, in the overall range of compositions ($0 \leqslant x \leqslant 1$). The SP methodology has been adopted and adapted for the growth of $Mg_xZn_{1-x}O$ QDs because it is one of the most inexpensive, simple and easily scalable techniques used for the deposition of semiconductor, metal oxide thin films and nanostructures.[23–25] Compared with other current epitaxial growth technology, SP technique would benefit the industrial scale production. To date no reports have been published, to the best of our knowledge, on the growth of $Mg_xZn_{1-x}O$ quantum dots on substrates in the overall range of Mg concentration ($0 \leqslant x \leqslant 1$), and hence this work opens up a new way for obtaining the QDs and application of these QDs in devices operating in the UV range.

Experimental

Magnesium zinc oxide nanoparticles were deposited onto pre-heated substrates with various crystal structures (hexagonal c-sapphire, cubic Si (100) and amorphous quartz) from solid free zinc diacetate dihydrate ($Zn(CH_3COO)_2 \cdot 2H_2O$) and magnesium acetate ($Mg(CH_3COO)_2 \cdot 4H_2O$) (Fisher Scientific, Laboratory reagent grade) solution dissolved in methanol (Scharlau, reagent grade). Composition of Mg in the $Mg_xZn_{1-x}O$ nanoparticles is controlled by adjusting the Mg concentration (magnesium acetate) in the starting precursor solution. From the previous study on ZnO QDs we have selected a set of experimental conditions in order to obtain a narrow range of sizes and densities.[23] Precursor concentration of 0.0125 M and growth temperature of 315 °C were used for depositing the QDs. The atomised precursor, generated by means of a spray nozzle, was sprayed onto the substrates using nitrogen as carrier gas (99.999%). The rate of spray was kept constant at 14.7 ml min^{-1} while the substrate to nozzle distance was kept constant for the experiments at 28 cm, so that a uniform spray of about 21 cm in diameter span arrived at the substrate. The morphology of the samples was studied by using a Hitachi S-4800 field emission electron microscope (acceleration voltage: 30 kV). A conductive layer of gold–palladium was deposited over the QDs using dc-sputtering prior to the scanning electron microscopy (SEM) analysis. The thickness of gold-palladium coating was about 1 nm, so that an increase in size of about 2 nm of $Mg_xZn_{1-x}O$ QDs covered by the coating is expected. High resolution transmission electron micrographs (HR-TEM), energy dispersive X-ray analysis (EDAX) and selected area electron diffractions (SAED) were recorded with a Tecnai G2 F20 field emission gun transmission electron microscope under an acceleration voltage of 200 kV. For TEM-EDAX and SAED measurements, $Mg_xZn_{1-x}O$ QDs were deposited on TEM support carbon film on copper grid substrates (C-grid) placed over a heated c-sapphire substrate. Particle size and morphology of the $Mg_xZn_{1-x}O$ QDs were studied by analysing over 200–300 particles from HR-TEM. Fast Fourier transform (FFT) performed on HRTEM recorded from QDs were used to determine

Table 1 Range of compositions, sizes and some details of the $Mg_xZn_{1-x}O$ nanoparticles obtained by using different growth techniques

Serial No.	Authors	Range of 'x'	Growth technique	Substrate	Cubic (C)/Hexagonal (H)
1.	Manoranjan et al.[16] (size: 10–12 nm)	$0 \leqslant x \leqslant 0.17$ $x \geqslant 0.2$	Solution route	—	H Mixed phase
2.	Manuel et al.[21] (size: 95–172 nm)	$0 < x < 0.19$ $x \geqslant 0.19$	Polymer based method	—	H Mixed phase
3.	Guangqiang et al.[20] (size: 20–50 nm)	$0 < x < 0.21$ $0.21 \leqslant x \leqslant 0.73$ $x \geqslant 0.82$	Polymer based method	—	H Mixed phase C
4.	Xianyong et al.[22] (size: 180 nm)	$x = 0.3$	Sono-chemical method	—	H
5.	John et al.[18] (size: 40 nm)	$x \leqslant 0.3$ $x > 0.3$	Thermal decomposition	—	H Mixed phase
6.	Zeng et al.[15] (size: 9 nm)	$x = 0.01$ and 0.23	LP-MOCVD	Si	H

the crystal structure of the $Mg_xZn_{1-x}O$ QDs. TEM-EDAX spectra were recorded from $Mg_xZn_{1-x}O$ QDs by using an EDAX-AMETEK detector and composition of the $Mg_xZn_{1-x}O$ QDs was determined. X-ray photoelectron spectroscopy (XPS) measurements of ZnO and $Mg_xZn_{1-x}O$ QDs were performed in an ultra-high vacuum system ESCALAB210 (base pressure 1.0 × 10^{-10} mbar) from Thermo VG Scientific. The samples were fixed onto the sample holder and a contact was made from the sample surface to the holder by means of silver paint to prevent the sample from becoming extensively charged while emitting electrons. The measurements were taken over an area of 1 mm². Photoelectrons were excited by using the Al Kα line (1.4866 keV). As a reference in the binding energy, we used the C 1s peak (fixed to 285 eV). XPS compositional analyses were performed on $Mg_xZn_{1-x}O$ QDs grown on sapphire substrate (Mg concentration: 0 to 100%) by considering empirical atomic sensitivity factors of the Mg 1s and Zn 2p core levels.[26] Thus the atomic sensitivity factor of the Mg 1s core level was found to be 3.5 when photoelectrons are excited by the Al Kα line.[26] Nevertheless, available atomic-sensitivity-factor value for the Zn 2p$_{3/2}$ core level (4.8) was related to photoelectrons excited from this level by using a Mg Kα line. Taking in mind that we have excited with the Al Kα line, the use of that atomic-sensitivity-factor value for the Zn 2p$_{3/2}$ core level limits, a little bit, the quantitative accuracy, in particular in the middle and Zn-rich composition regions. Finally, the room temperature absorption coefficient has been estimated for the $Mg_xZn_{1-x}O$ QDs deposited on quartz using a Jasco V650 spectrophotometer working in transmission mode. A reference quartz template without $Mg_xZn_{1-x}O$ QDs has been measured and the signal subtracted from the $Mg_xZn_{1-x}O$ spectra. The spectrophotometer covers the 200 to 800 nm spectral region by using a deuterium and a halogen lamp, and thus nominally allows the analysis of material with band gap energies up to ~6–6.5 eV.

Results and discussion

Scanning electron microscopy (SEM) analysis

As said before, on the basis of the previous study on ZnO QDs we have fixed precursor concentration and growth temperature to obtain $Mg_xZn_{1-x}O$ QDs of sizes in the range of ~4–6 nm, and densities in the order of ~10^{11} QD cm^{-2} to cover about ~13% of the substrate.[23] Representative scanning electron micrographs are depicted in Fig. 1–3. As a first finding, the study shows that under the experimental conditions here chosen, the $Mg_xZn_{1-x}O$ QDs can be grown irrespective of the crystal structure of the substrate (c-Al_2O_3, Si (100) and amorphous quartz), without any significant difference in the morphological characteristics of the QDs. The most probable reason to obtain similar surface morphology irrespective of the crystal structure of the substrate may be due to the growth of QDs over a wetting layer, which is formed underneath the QDs [23]. Uniform and well isolated $Mg_xZn_{1-x}O$ QDs ranging between ~4–6 nm in size, densities in the range of ~10^{11} QDs cm^{-2} and a Mg nominal concentration between 0 and 40%

over c-Al_2O_3 substrate can be seen in Fig. 1a and b (and on silicon in Fig. 2a and b). For Mg nominal concentrations ⩾50%, and maintaining same growth conditions, a decrease in the QD density and size was observed (due to decrease of growth rate). Hence to obtain QDs of similar size and densities, growth time was varied between 1 and 4 minutes for growth in the range of Mg concentrations $0.09 < x < 0.81$, whereas a growth time of 6 minutes was used for the growth of MgO QDs.

Structural characterisation of $Mg_xZn_{1-x}O$ QDs

Taking into account the low influence of the substrate (Si (100), c-Al_2O_3, quartz and glass)[23] on the morphological properties of ZnO QDs under the experimental conditions used in this study, TEM and SAED analysis of the $Mg_xZn_{1-x}O$ QDs with various Mg concentrations were performed on samples deposited over carbon-grid substrates, maintaining similar growth conditions. Fig. 4 and 5 depict the TEM images of $Mg_xZn_{1-x}O$ QDs grown over C-grid with Mg concentrations ranging from 0 to 50% and 70 to 100% (nominal), respectively. Uniform and isolated QDs of sizes in the range of 2–4 nm can be observed from the TEM micrographs (Fig. 4 and 5). It is worth to note that the QDs size measured using SEM image gives an overestimated value due to the Au–Pd coatings and SEM microscope's resolution.[27]

SAED spectra were recorded on those samples deposited over C-grid substrates (Mg nominal concentration: 0 to 100%) and the electron diffraction rings were indexed (Fig. 6). The radius of the electron diffraction ring $r(hkl)$ and the inter-planar lattice spacing $d(hkl)$ are related by $r(hkl) \times d(hkl) = L\lambda$, where $L\lambda = 1$ is the camera constant of the transmission electron microscope. From the electron diffraction pattern, r is measured and the lattice spacing d is determined. The experimental d-values determined from the SAED pattern of $Mg_{0.0}Zn_{1.0}O$ (ZnO) QDs are 2.819, 2.6319, 2.5100, 1.9500, 1.6630, 1.5065 and 1.4050 Å corresponding to the planes (100), (002), (101), (102), (110), (103) and (200) respectively, which are indexed as the wurtzite phase of ZnO (JCPDS: 36-1451) with space group $P63mc$ (Fig. 6a). It is worth noticing that no diffraction rings corresponding to metallic Zn, Mg or any other impurities are observed, showing the purity of the $Mg_xZn_{1-x}O$ QDs grown using SP. Similarly, the electron diffraction rings recorded from the $Mg_{1.0}Zn_{0.0}O$ (MgO) QD samples were indexed to the cubic MgO (space group $Fm3m$) (Fig. 6f). The d-values determined from the MgO QD sample were 2.5608, 2.2078, 1.5873, 1.2944, 0.9732 and 0.8933 Å corresponding to the planes (111), (200), (220), (311), (331) and (422) respectively (JCPDS: 045-0946).

Careful analysis of electron diffraction patterns for the $Mg_xZn_{1-x}O$ QD samples reveals that only diffraction rings corresponding to the hexagonal alloy $Mg_xZn_{1-x}O$ are present up to a Mg nominal concentration of 45%. No diffraction rings from the MgO phase were observed in SAED patterns, indicating that the material ($Mg_xZn_{1-x}O$) is present only in its hexagonal phase (single phase) and magnesium has been incorporated into the ZnO lattice. Onset of Mg content (in the precursor solution) about 50% resulted in appearance of additional diffraction rings along (200) and (220) planes corresponding to the cubic $Mg_xZn_{1-x}O$ alloy, showing co-
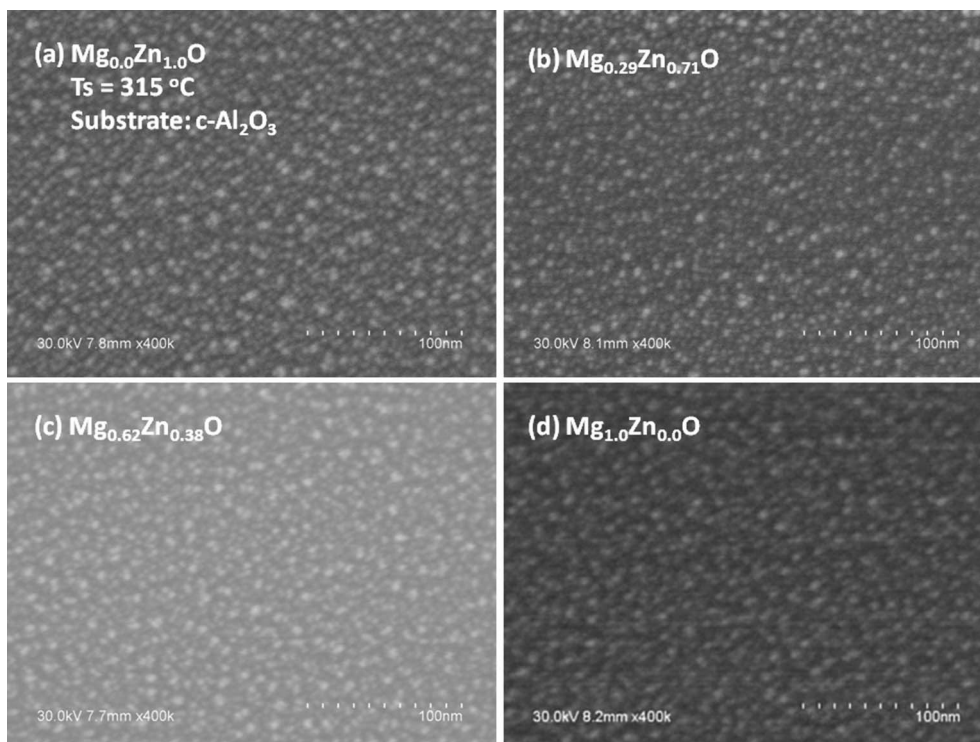
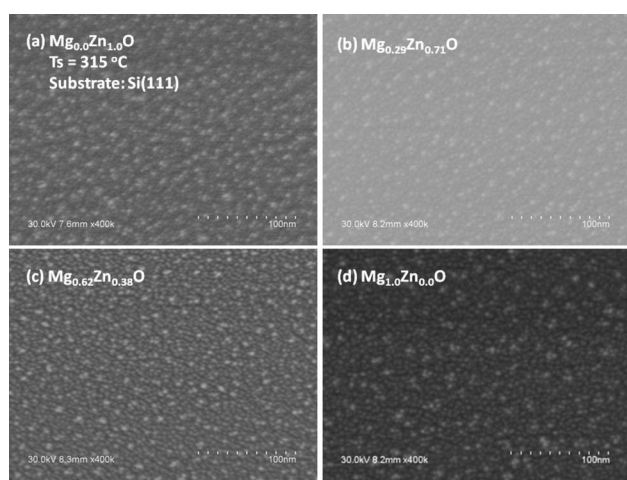**Fig. 1** SEM micrographs of $Mg_xZn_{1-x}O$ QDs grown on c-Al_2O_3 with Mg concentration (nominal) (a) 0%, (b) 40%, (c) 80% and (d) 100% at a growth temperature of 315 °C.

existence of hexagonal and cubic phases of the QDs in the range 50 to 85%. Further increase in Mg concentration to values greater than or equal to 90% in the precursor solution results in the growth of a single phase cubic alloy with characteristic electron diffraction rings of the cubic $Mg_xZn_{1-x}O$. All the diffraction rings corresponding to hexagonal phase of $Mg_xZn_{1-x}O$ were absent for those nominal concentrations higher than 90% (showing a complete phase transition from hexagonal $P63mc$ space group to cubic $Fm3m$ space group).

High resolution TEM characterization has been used to have a close look at the crystalline properties of the $Mg_xZn_{1-x}O$ QDs. Fig. 7a depicts the HRTEM micrograph of the $Mg_{0.21}Zn_{0.79}O$ nanoparticles (nominal concentration of Mg: 30%), whereas Fig. 7b shows the magnified HRTEM image of one nanoparticle (see Fig. 7a). The inter-planar distance measured from the HRTEM image is in good agreement with the values determined using SAED analysis. Fast Fourier transform (FFT) performed in the selected nanoparticle shows the associated hexagonal crystal structure (Fig. 7c). Similar FFT study conducted of $Mg_{0.81}Zn_{0.09}O$ shows the cubic crystal structure corresponding to this composition (Fig. 8c). However, one can clearly distinguish the cubic and hexagonal phases of $Mg_xZn_{1-x}O$ alloy from HRTEM (Fig. 7b and 8b) and FFT (Fig. 7c and 8c) images. Thus by using HRTEM and FFT

Fig. 2 SEM micrographs of $Mg_xZn_{1-x}O$ QDs grown on Si (100) with Mg concentration (nominal) (a) 0%, (b) 40%, (c) 80% and (d) 100% at a growth temperature of 315 °C.
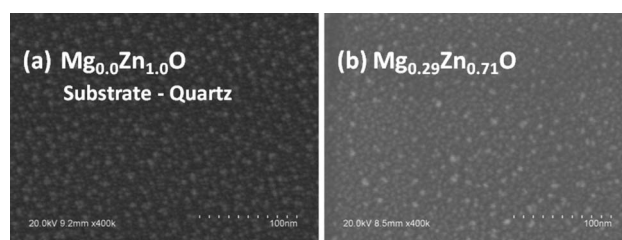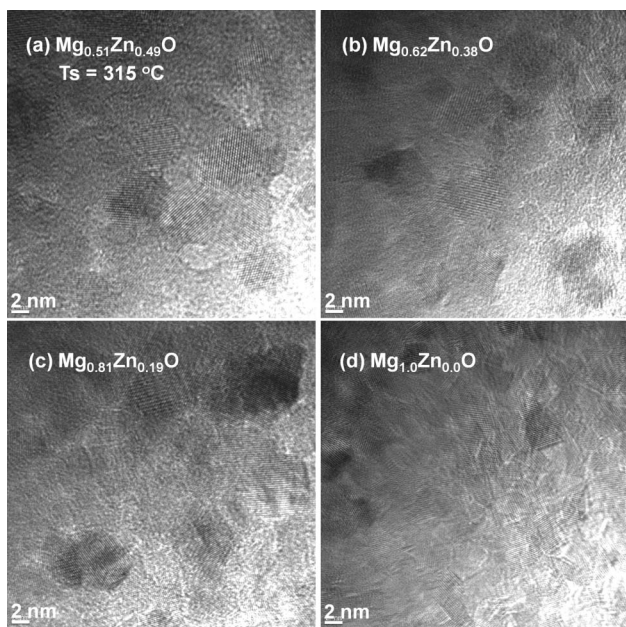

Fig. 3 SEM micrographs of $Mg_xZn_{1-x}O$ QDs grown on quartz with Mg concentration (nominal) (a) 0% and (b) 40%.
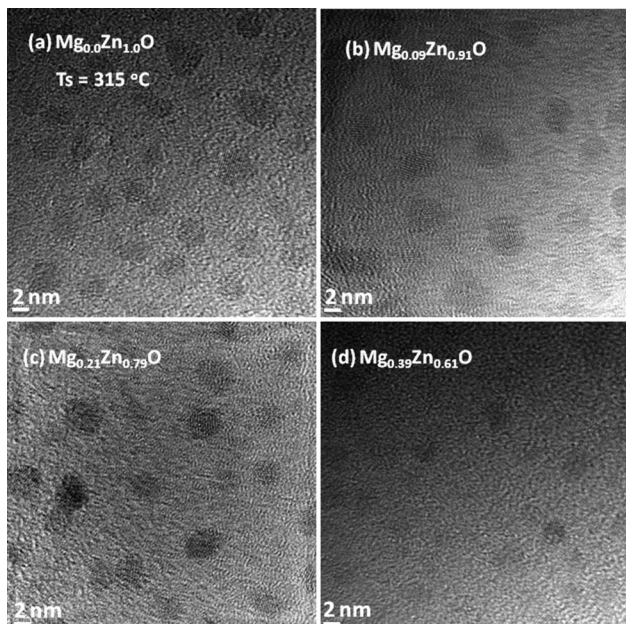
Fig. 4 TEM images of $Mg_xZn_{1-x}O$ QDs grown on C-grid with Mg nominal concentration (a) 0%, (b) 10%, (c) 30% and (d) 50% at a growth temperature of 315 °C.

analysis it is possible to identify and distinguish the $Mg_xZn_{1-x}O$ QDs of various crystal structures. The HRTEM profile of cubic $Mg_xZn_{1-x}O$ thin film reported by Liang *et al.* closely matches with the profile obtained in the present study from cubic $Mg_xZn_{1-x}O$ QDs.[28] In brief, high resolution TEM and SAED analysis proved that the hexagonal symmetry of the

Fig. 5 TEM images of $Mg_xZn_{1-x}O$ QDs grown on C-grid with Mg nominal concentration (a) 70%, (b) 80%, (c) 90% and (d) 100% at a growth temperature of 315 °C.

$Mg_xZn_{1-x}O$ are preserved/maintained up to a Mg nominal concentration of 45% ($x \leqslant 0.32$) and Mg substitution does not lead to any change in crystal structure.

Effect of Mg incorporation

Compositional analysis of $Mg_xZn_{1-x}O$ QDs was carried out using XPS as well as TEM-EDAX measurements. TEM-EDAX spectra were recorded from $Mg_xZn_{1-x}O$ QD samples deposited on C-grid, whereas XPS compositional analyses were performed on $Mg_xZn_{1-x}O$ QDs grown on sapphire substrate (Mg concentration: 0 to 100%). Fig. 9 shows the evolution of measured atomic concentration of Mg from $Mg_xZn_{1-x}O$ QD samples (determined using EDAX and XPS) as a function of magnesium nominal concentration in the starting precursor solution. As the concentration of Mg in the precursor solution was increased, the actual Mg content in $Mg_xZn_{1-x}O$ QDs was gradually enhanced; however the actual concentration of Mg in the samples was less than the nominal concentration in the precursor solution. The low efficiency of Mg incorporation into ZnO lattice is an experimental fact due to the solubility limit of Mg in the hexagonal ZnO lattice. The hexagonal crystal structure of ZnO does not have atomic/Wyckoff positions to accommodate the excess Mg atoms supplied from the precursor solution, and hence the Mg atoms compete with the lattice to modify the crystal structure (from hexagonal to cubic) for accommodating higher number of Mg atoms. In a hexagonal ZnO unit cell there are two tetrahedrally-coordinated (T_d) Zn atoms, whereas in cubic MgO unit cell there are four octahedrally-coordinated (O_h) Mg atoms.

However, $Mg_xZn_{1-x}O$ QDs grown with Mg concentrations lower than 45% (nominal) were able to accommodate the Mg in a single hexagonal phase. Nevertheless on increasing the Mg concentration to a value of 50% (nominal), cubic phase of $Mg_xZn_{1-x}O$ appeared in the SAED spectrum, Fig. 6c. In fact, onset of the Mg concentration about 50% forces the hexagonal lattice to undergo a phase transition to cubic phase in order to accommodate more number of Mg atoms. Further increase of Mg concentration higher than 50% (nominal) resulted in a continuous increase in the overall Mg concentration (actual).

The lower Mg incorporation in ZnO QD (Mg concentration in the range 10 to 50% (nominal) can be understood in the frame of the lower impurity solubility limit in nanocrystals/QDs in accordance with the ''self-purification'' model proposed by Gustavo *et al.*[29] One of the major factors that limits the doping efficiency or alloying of nanoparticles is the surface binding energy of the dopant atoms on the individual nanocrystals surface. It has been demonstrated in a classical paper by Steven *et al.* that the doping efficiency is determined by the binding energy of the dopant atoms on the individual nanocrystals surface.[30] The surface binding energy for wurtzite nanocrystals is three times less than that of zinc-blende or rock-salt structures on (001) faces.[16,30] Therefore in the present study, it seems that the lower incorporation of Mg in ZnO lattice with respect to the nominal concentration of Mg in the starting precursor solution is also related to the crystal structure of ZnO, in addition to other limits in the miscibility as could be inferred from the phase diagram corresponding to the alloy as a bulk crystal.[31] Hence during the growth of $Mg_xZn_{1-x}O$ (at lower Mg concentrations) all the Mg atoms
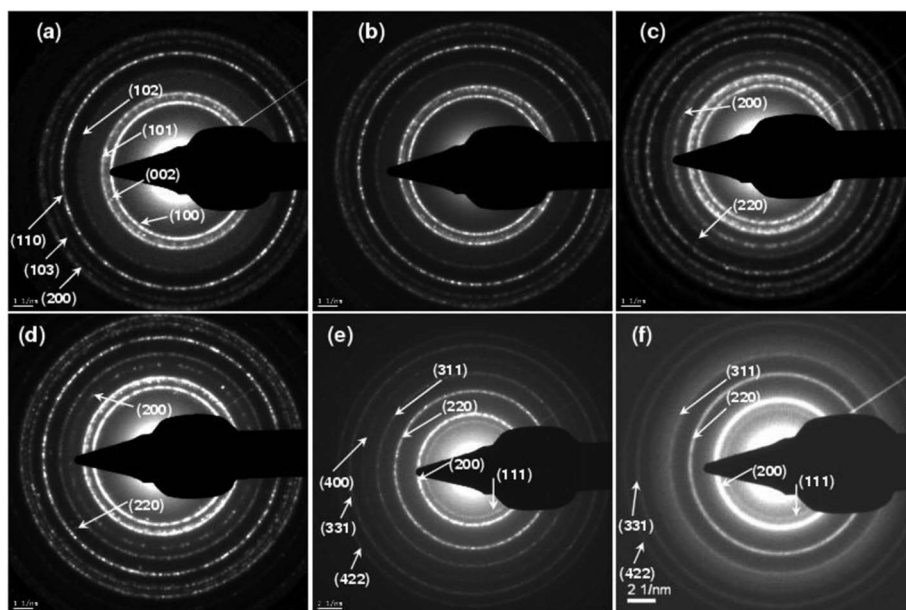
Fig. 6 SAED patterns recoded from $Mg_xZn_{1-x}O$ QDs samples deposited on C-grid with Mg concentration (a) 0%, (b) 30%, (c) 50%, (d) 70%, (e) 90% and (f) 100%.

supplied from the precursor are not bound/incorporated to the lattice, and eventually get desorbed from the lattice resulting in the formation of $Mg_xZn_{1-x}O$ QDs with lower Mg concentration (with respect to the concentration in precursor solution). Unlikely, if we consider the incorporation of Zn in MgO lattice (cubic), the efficiency is higher, which resulted in the growth of $Mg_{0.91}Zn_{0.09}O$, $Mg_{0.81}Zn_{0.19}O$ and $Mg_{0.62}Zn_{0.38}O$ with a Zn

concentration of 5, 10 and 20% in the starting precursor solution.

From the inter-planar distance (d-values) determined by means of SAED analysis, lattice parameters of hexagonal ("a"and "c") and cubic ("a") phases of $Mg_xZn_{1-x}O$ QDs were determined using the following relation, respectively:[32]

$$Hexagonal : \frac{1}{d^2} = \frac{4}{3}\left(\frac{h^2+hk+k^2}{a^2}\right) + \frac{l^2}{c^2}$$

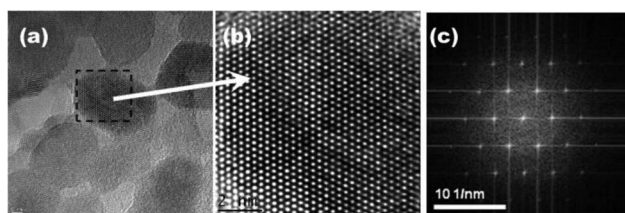$$Cubic : \frac{1}{d^2} = \frac{h^2+k^2+l^2}{a^2}$$

Fig. 7 (a) HRTEM image of $Mg_{0.21}Zn_{0.79}O$ nanoparticles, (b) enlarged HRTEM image of one nanoparticle (grain size about 8–10 nm) and (c) FFT of the selected NP showing their mono crystallinity in hexagonal structure.
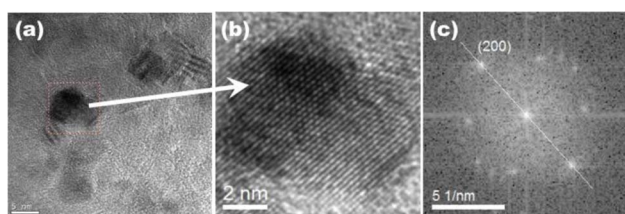

Fig. 8 (a) HRTEM image of $Mg_{0.81}Zn_{0.19}O$ nanoparticles, (b) enlarged HRTEM image of one nanoparticle (grain size about 8–10 nm) and (c) FFT of the selected NP showing their mono crystallinity in cubic phase structure.
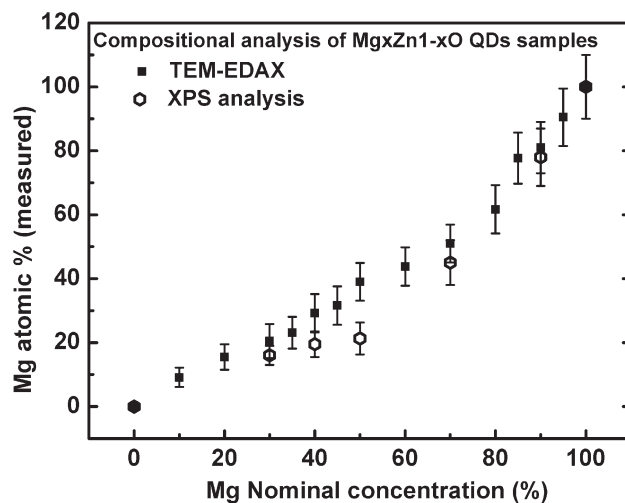

Fig. 9 Evolution of magnesium content in $Mg_xZn_{1-x}O$ QD samples (determined using TEM-EDAX and XPS) as a function of Mg nominal concentration in the starting precursor solution.

Fig. 10a shows the evolution of the "a" and "c" lattice parameters of the hexagonal alloy $Mg_xZn_{1-x}O$ with Mg nominal concentration ranging from 0 to 100%. To determine "a" and "c" lattice parameters of the hexagonal QDs, electron diffraction rings corresponding to the (100) and (103) planes were used, whereas "a" lattice constant of cubic $Mg_xZn_{1-x}O$ QDs was determined using the (200) electron diffraction ring. Standard value of "a" and "c" lattice parameters of ZnO with hexagonal wurtzite structure are 3.2498 Å and 5.2066 Å respectively (JCPDS: 36-1451). In the basis of the present study, we can observe an increase in the a-lattice parameter and a decrease in c-lattice parameter of hexagonal alloy $Mg_xZn_{1-x}O$ QDs upon increasing the Mg concentration. The variation in the value of lattice parameters recorded from $Mg_xZn_{1-x}O$ QD samples has been reported as clear evidence of the substitution of Zn^{2+} sites by Mg^{2+} in ZnO lattice to form a $Mg_xZn_{1-x}O$ alloy.[11,21,33] The a-lattice parameter gradually increased with increase in Mg concentration up to 30% (measured value $x = 0.21$), thereafter the change in the lattice constant with increase in nominal Mg concentration was very small up to Mg concentration of 50%. The small change in lattice constant observed near the Mg concentration range where the secondary cubic phase appeared (50% nominal) indicated that the incorporation of Mg in ZnO lattice is very low in this concentration range. However further increase in the Mg concentration to 70 and 80% (nominal), exhibited wide change in a-lattice constant. A similar behavior was observed in the case of c-lattice constant, where the c-lattice constant decreased on increasing Mg concentration. This increase in the a-lattice constant (and decrease in c-lattice constant) is attributed to the hexagonal-to-cubic phase transition undergone on increasing the Mg concentration. However the presence of mixed phases (hexagonal and cubic) limits us to determine the actual stoichiometry of the sample at which the phase transition occurs. The variation in lattice parameter that appears on varying the Mg concentration is due to the substitution of tetrahedrally co-ordinated (T_d) Zn^{2+} sites by

Mg^{2+}. However due to smaller ionic radius of Mg^{2+}, substitution of Zn^{2+} by Mg^{2+} force the c-lattice parameter to shrink due to the strain exerted by the Mg substitution on the ZnO lattice upon increasing the Mg concentration.[11,16,34] Similarly a corresponding elongation of a-lattice parameter is observed in ref. 21 and 32. Likewise, introducing Zn to the cubic MgO lattice resulted in substitution of octahedrally co-ordinated (O_h) Mg^{2+} by Zn^{2+} and a reduction in a-lattice parameter is observed (Fig. 10b), which is attributed to the distortion of the parent cubic MgO structure upon Zn incorporation. In addition a saturation of a-lattice parameter is observed in the mixed phase region, due to the solubility limit of Zn in cubic MgO lattice. When Mg is introduced into ZnO lattice, at an amount higher than 32 at%, ZnO starts to dissolve in the MgO matrix. Under such circumstances, mixed phases of cubic and hexagonal $Mg_xZn_{1-x}O$ co-exist. This is in accordance with the reported values of phase separation observed in $Mg_xZn_{1-x}O$ nanocrystals (>30 at%) by John et al.[18] However Manoranjan et al.,[16] Manuel et al.[21] and Guangqiang et al.[20] observed phase separation at about $x \geqslant 0.2$ in $Mg_xZn_{1-x}O$ nanocrystals. The differences in the value of Mg concentration in which the phase separation appears point to the influence of growth method, presence or absence of a substrate and QDs size. It is worth noticing that the c-lattice constant of the $Mg_xZn_{1-x}O$ QDs ($x = 0$) observed in the present study (Fig. 10a) is higher than the standard value of hexagonal ZnO due to the surface stress on the ZnO nanocrystals. The stress causes a high lattice strain and leads to lattice expansion in order to relieve the strain.[35] This fact indicates that in the $Mg_xZn_{1-x}O$ QDs grown using spray pyrolysis method, the stress relaxes elastically. Sameer et al. demonstrated in CeO_2 nanoparticles (size 3 to 150 nm) that the surface stress induced by reduction in particle size modifies the lattice constant in a wide range.[35] Similarly the cubic MgO QD also exhibited a higher value of a-lattice constant with respect to the standard bulk cubic MgO ($c = 4.2112$ Å) (Fig. 10), as a new evidence of the fact that the reduction in crystallite size influences the lattice constant of $Mg_xZn_{1-x}O$ QDs.

X-ray photoelectron spectroscopy analysis

To understand the effect of the incorporation of Mg^{2+} and Zn^{2+} on the electronic properties of ZnO and MgO QDs, respectively, the chemical state of the Zn and Mg in $Mg_xZn_{1-x}O$ QDs was analyzed by using XPS. Fig. 11 shows the Zn 2p and Mg 1s core level spectra recorded from $Mg_xZn_{1-x}O$ QDs ($0 \leqslant x \leqslant 1$). We have selected precisely these two core-level regions due to the fact that the atomic species of interest (Mg and Zn) separately contributes to the photoemission signal detected in each one of these regions, contrary to that occurring for the Mg 2s core-level region. The Zn 2p core level measured in ZnO QDs (Fig. 11a) exhibits two peaks corresponding to the spin–orbit doublet of the Zn 2p level. A two-peak Gaussian fit of this doublet reproduces the experimental spectrum, giving a spin–orbit splitting value of 23.0 eV and a binding energy (BE) of the Zn $2p_{3/2}$ core level (1023.2 eV) that is in accordance to that usually reported for ZnO.[22,28] The Mg 1s core level measured in MgO QDs (Fig. 11b) shows a feature reproduced by the fitting of an unique Gaussian peak located at 1305.2 eV. On the one hand, incorporation of Mg to ZnO (QDs) lattice appears to shift
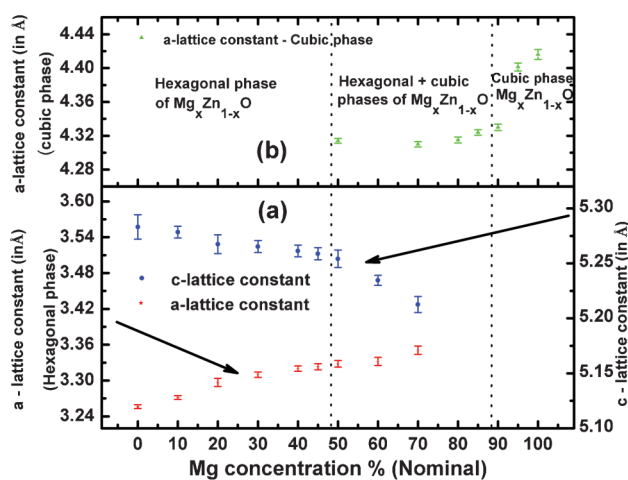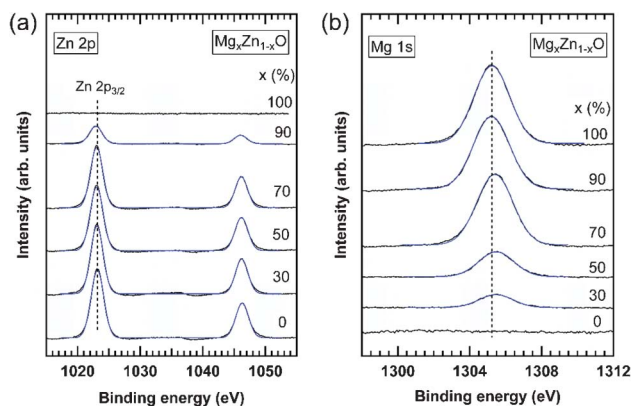

Fig. 10 Evolution of the lattice parameters of (a) hexagonal and (b) cubic magnesium zinc oxide alloy QDs as a function of magnesium concentration. The lines are drawn just to guide the reader's eyes.
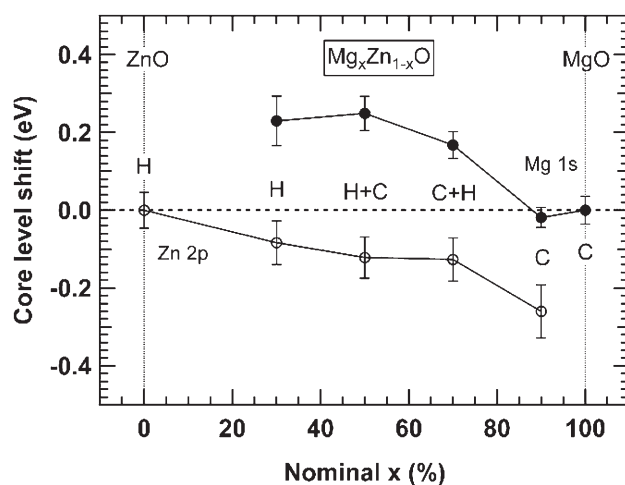
Fig. 11 XPS spectra of (a) Zn 2p and (b) Mg 1s core levels measured in $Mg_xZn_{1-x}O$ QDs grown on c-Al_2O_3. The nominal Mg concentration of the QDs is indicated on each curve. Solid blue lines are Gaussian fitting of the experimental results. Vertical dashed lines in each plot indicate the energy position of the Zn $2p_{3/2}$ and Mg 1s core levels in ZnO and MgO QDs, respectively, as obtained by the fitting of the XPS spectra.

Fig. 12 Shift of the Zn 2p (open circles) and Mg 1s (filled circles) core levels measured in $Mg_xZn_{1-x}O$ QDs, with respect to these recorded in ZnO and MgO QDs, respectively. These shifts have been obtained by Gaussian fitting of the experimental spectra and the error bars are the standard deviation of the fitting parameters. To guide discussion, we have indicated the structure of the $Mg_xZn_{1-x}O$ QDs [hexagonal (H), cubic (C), or mixed phases (C + H)].

the Zn 2p doublet to lower BE. On the other hand, incorporation of Zn to MgO (QDs) lattice seems to shift the Mg 1s core level to higher BE. In both cases, no trace from metallic Zn or Mg (cation segregation) was detected, which would support the substituting behavior between cations evidenced by SAED results. Moreover, the Mg 1s and Zn 2p core levels measured in $Mg_xZn_{1-x}O$ QDs ($0 < x < 1$) seemed not to show traces from additional peaks different from these detected in MgO and ZnO QDs. These facts suggest that a fitting procedure similar to that already performed for ZnO and MgO QDs can be adopted to analyze the core level spectra measured in $Mg_xZn_{1-x}O$ QDs. The results of these fittings indicate that Mg (Zn) incorporation into ZnO (MgO) lattice tends to shift the core levels of the starting materials without an appreciable increasing of the peak width. Fig. 12 summarizes the value of the core-level shift, with respect to these of ZnO and MgO QDs, which has been observed in $Mg_xZn_{1-x}O$ QDs, as a function of the nominal Mg content. From these results, it can be seen that the progressive incorporation of Mg into $Mg_xZn_{1-x}O$ QDs not only alters the atomic configuration of the QDs but also gradually tunes their electronic structure. In this respect, it is interesting to notice some aspects of the electronic structure of purely cubic and tetrahedral $Mg_xZn_{1-x}O$ QDs. The Mg atoms incorporated into the tetrahedral lattice of $Mg_{0.32}Zn_{0.68}O$ QDs show a Mg 1s core level shifted by 0.24 eV to higher BE with respect to these in cubic MgO. On the other hand, Zn atoms incorporated into the cubic lattice of $Mg_{0.81}Zn_{0.19}O$ QDs show a Zn 2p core level shifted by 0.24 eV to lower BE with respect to these in tetrahedral ZnO. This evidence indicates that the cation on-site potential established, mainly, by the surrounding oxygen atoms in $Mg_xZn_{1-x}O$ QDs with a octahedral cubic configuration is 0.24 eV more repulsive than that of QDs with a tetrahedral configuration and independent of the cation choice (Mg or Zn). The more negative cation on-site potential created in the cubic configuration can be readily understood in terms of the cation coordination number: An octahedral cubic-coordinated

cation must donate 1/3 electrons per bond whereas a tetrahedral-coordinated cation must donate 1/2 electrons per bond. Therefore, the higher charge-transfer degree of the tetrahedral bonds relatively depopulates (of electrons) their corresponding cations, increasing the BE of photoelectrons excited from these cations with respect to the octahedral cubic-coordinated ones. The valence band of MgO and ZnO is composed by states with O 2p orbital character and the conduction band is formed by cation s-orbitals. In these compounds, the Zn 4s and Mg 3s states differ from the valence band by 3.4 and 7.6 eV, respectively. Therefore, assuming a rigid band model of the band alignment and taking into account that the on-site cation potential changes by -0.24 eV in going from the tetrahedral to the cubic configuration, it would be expected that substitutional Mg in ZnO QDs introduced s-states well inside the ZnO conduction band (around 4 eV above the conduction band minimum) that would tend to increase the band gap of hexagonal $Mg_xZn_{1-x}O$ QDs in so far the magnesium content increase due to the shifting to higher energies of the conduction band density of states. Conversely, substitutional Zn incorporated into MgO would be expected that introduces s-states in the midgap of MgO (around 4 eV below the conduction band minimum) that would naturally tend to reduce the band gap of cubic $Mg_xZn_{1-x}O$ QDs as the Zn content increases.

Optical characterisation

Optical absorption spectra in the wavelength range of 250–800 nm were recorded at room temperature from $Mg_xZn_{1-x}O$ QDs deposited on transparent quartz substrates. Samples with Mg concentrations ranging from 0 to 40% Mg (nominal values) were measured in transmission mode (Fig. 13), and the onsets to the optical absorption coefficient extracted from a linear extrapolation of the initial absorption slope. In this study we have focused on this range of magnesium content in which
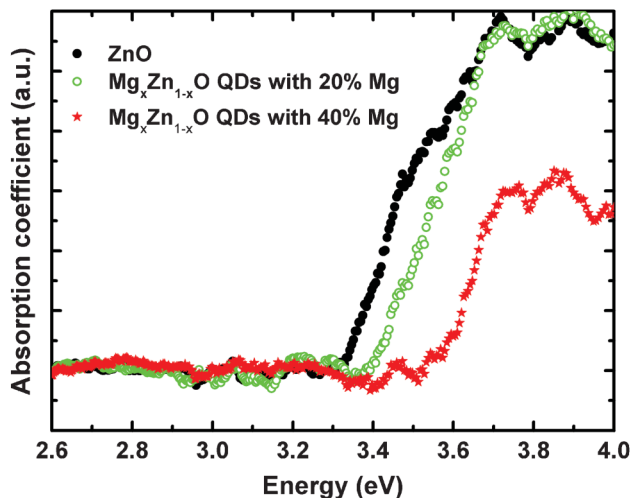
Fig. 13 Absorption spectra of $Mg_xZn_{1-x}O$ QDs deposited on quartz substrate with various Mg concentrations.

only a single hexagonal phase of $Mg_xZn_{1-x}O$ is present, avoiding disturbing effects due to the existence of mixed phases with undetermined singular composition.

As we can clearly observe in Fig. 13, the onset of the absorption coefficient, which approximately corresponds to the optical energy gap, shifted as a function of the Mg content from 0 to 40%, which is clear evidence of substitution of Zn^{2+} by Mg^{2+} in the ZnO lattice that yields an increase in the band gap energy. In order to confirm that the observed optical absorption actually results from the QDs and not from the wetting layer forming underneath, a sample was prepared only containing a wetting layer equivalent to that with the 40% Mg QDs (chosen to be representative sample of the series), but with no QDs on the surface. As seen in Fig. 14 the wetting layer by itself does not produce a measurable optical absorption. Thus, we can univocally assign the observed optical absorption coefficients to the wurtzite $Mg_xZn_{1-x}O$ QDs formed on the
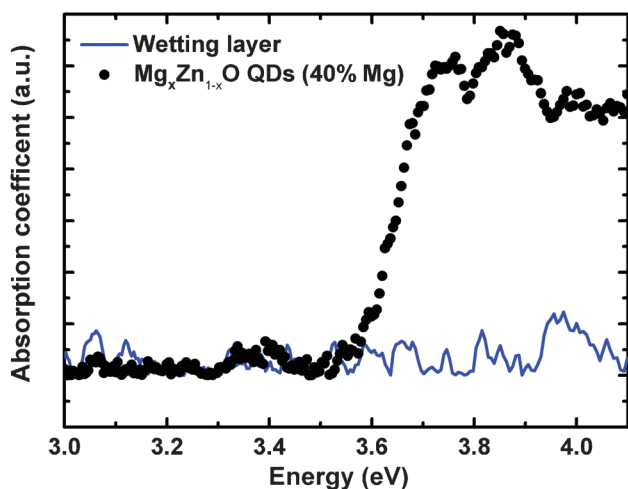

Fig. 14 Absorption spectra of $Mg_xZn_{1-x}O$ QDs and only wetting layer (without QDs) of same Mg content deposited on quartz substrate.

surface. Ning et al.[36] performed optical transmission studies on $Mg_xZn_{1-x}O$ nanoparticles (30 nm size) in the range $x = 0$ to 0.2. These nanoparticles have been grown via sol–gel technique and dip coated on quartz substrates. Similarly as in our results a relatively small blue shift in optical absorption edge was observed on increasing Mg content. Our preliminary optical characterization confirms the ability of the alloy to modify significantly the ZnO optical properties by adding controlled amounts of magnesium without changing the crystalline structure.

Conclusions

In summary, we have studied the growth of $Mg_xZn_{1-x}O$ QDs ($0 \leqslant x \leqslant 1$) on c-sapphire, Si (100) and quartz substrates by using the spray pyrolysis methodology. Composition of the Mg in $Mg_xZn_{1-x}O$ QDs is controlled by adjusting the Mg concentration in the starting precursor solution. The study proves that by controlling the Mg concentration from 0 to 45% ($0 \leqslant x \leqslant 0.32$, measured using TEM-EDAX) and 90 to 100% ($0.81 \leqslant x \leqslant 1$) the growth of single phase hexagonal $Mg_xZn_{1-x}O$ QDs or cubic $Mg_xZn_{1-x}O$ QDs can be successfully attained. The crystal structure suffer a phase transition from hexagonal to cubic structure on the onset of Mg concentration about 50%, which results in the growth of hexagonal and cubic phases of $Mg_xZn_{1-x}O$ in the intermediate range of Mg concentrations 50 to 85% ($0.39 \leqslant x \leqslant 0.77$). The study shows that the $Mg_xZn_{1-x}O$ QDs can be grown irrespective of the crystal structure of c-Al_2O_3 and Si (100) substrates, without any significant difference neither in the structural nor morphological characteristics of QDs. On the other hand, we have analysed the evolution of ''a'' and ''c''-lattice parameters of the hexagonal $Mg_xZn_{1-x}O$ QDs with the increase in Mg concentration and similarly of the ''a'' parameter in the cubic $Mg_xZn_{1-x}O$ QDs. The study reveals that the surface binding energy and the crystal structure of the nanocrystals influence the incorporation of foreign atoms into the host lattice of nanocrystals. XPS measurements show that the segregation of cations is under the detection limit of the experimental setup and confirmed the substitution of tetrahedrally-coordinated (T_d) Zn^{2+} by Mg^{2+} in the ZnO lattice. In addition to this, XPS results revealed that the core-level binding energies are determined by the structural properties and coordination of the QDs, irrespective of the cation. The optical measurements performed on $Mg_xZn_{1-x}O$ QDs exhibited the ability to tune the optical energy gap of the QDs to shorter wavelength of UV region, which is attributed to the substitution of Zn^{2+} by Mg^{2+} in the ZnO lattice. The ability, here shown, to obtain $Mg_xZn_{1-x}O$ QDs in an extended-range of concentrations on different substrates paves the way for additional studies that can shed light on the potential of the alloy in a zero dimensional configuration for devices operating in the UV region.

Acknowledgements

References

1 K. Satoshi, S. Charles, H. Katsuyuki, G. Stephan, Y. Yoshihisa and A. Yasuhiko, *Nat. Mater.*, 2006, **5**, 887.

2 T. Thomay, T. Hanke, M. Tomas, F. Sotier, K. Beha, V. Knittel, M. Kahl, K. M. Whitaker, D. R. Gamelin, A. Leitenstorfer and R. Bratschitsch, *Opt. Express*, 2008, **16**, 9791.

3 L. Jang-Sik, C. Jinhan, L. Chiyoung, K. Inpyo, P. Jeongju, K. Yong-Mu, S. Hyunjung, L. Jaegab and C. Frank, *Nat. Nanotechnol.*, 2007, **2**, 790.

4 L. Kuo-Feng, C. Hsin-Ming, H. Hsu-Cheng, L. Li-Jiaun and H. Wen-Feng, *Chem. Phys. Lett.*, 2005, **409**, 208.

5 A. Ohtomo, M. Kawasakia, Y. Sakuraib, I. Ohkuboc, R. Shirokia, Y. Yoshidab, T. Yasudad, Y. Segawad and H. Koinumal, *Mater. Sci. Eng., B*, 1998, **56**, 263.

6 A. Tsukazaki, A. Ohtomo, T. Onuma, M. Ohtani, T. Makino, M. Sumiya, K. Ohtani, S. F. Chichibu, S. Fuke, Y. Segawa, H. Ohno, H. Koinuma and M. Kawasaki, *Nat. Mater.*, 2005, **4**, 42.

7 F. Shizuo, T. Hiroshi and F. Shigeo, *J. Cryst. Growth*, 2005, **278**, 264.

8 D. M. Bagnall, Y. F. Chen, Z. Zhu and T. Yao, *Appl. Phys. Lett.*, 1997, **70**, 2230.

9 Z. K. Tang, G. K. L. Wong, P. Yu, M. Kawasaki, A. Ohtomo, Y. Koinuma and Y. Segawa, *Appl. Phys. Lett.*, 1998, **72**, 3270.

10 J. Narayan, A. K. Sharma, A. Kvit, C. Jin, J. F. Muth and O. W. Holland, *Solid State Commun.*, 2002, **121**, 9.

11 W. I. Park, Y. Gyu-Chul and H. M. Jang, *Appl. Phys. Lett.*, 2001, **79**, 2022.

12 A. K. Sharma, J. Narayan, J. F. Muth, C. W. Teng, C. Jin, A. Kvit, R. M. Kolbas and O. W. Holland, *Appl. Phys. Lett.*, 1999, **75**, 3327.

13 X. Mingshan, G. Qinlin, W. Kehui and G. Jiandong, *J. Chem. Phys.*, 2008, **129**, 234707.

14 S. Choopun, R. D. Vispute, W. Yang, R. P. Sharma and T. Venkatesan, *Appl. Phys. Lett.*, 2002, **80**, 1529.

15 Y. J. Zeng, Z. Z. Ye, Y. F. Lu, J. G. Lu, L. Sun, W. Z. Xu, L. P. Zhu, B. H. Zhao and Y. Che, *Appl. Phys. Lett.*, 2007, **90**, 012111.

16 G. Manoranjan and A. K. Raychaudhuri, *J. Appl. Phys.*, 2006, **100**, 034315.

17 B. Leah, L. M. John, C. Xiang, H. Jesse and H. Heather, *Appl. Phys. Lett.*, 2006, **88**, 023103.

18 L. M. John, H. Jesse, H. Heather, C. Erin, M. James, B. Leah and N. M. Grant, *J. Appl. Phys.*, 2008, **104**, 123519.

19 H. Jesse, L. M. John, H. Heather, C. Erin, B. Leah, T. D. Pounds and M. G. Norton, *Appl. Phys. Lett.*, 2007, **91**, 111906.

20 L. Guangqiang, L. Ingo and W. Gerhard, *J. Am. Chem. Soc.*, 2006, **128**, 15445.

21 G. Manuel, R. Guillermo, A. Nuria and B. Salvador, *J. Appl. Polym. Sci.*, 2011, **119**, 2048.

22 L. Xianyong, L. Zhaoyue, Z. Ying and J. Lei, *Mater. Res. Bull.*, 2011, **46**, 1638.

23 R. Sreekumar, A. Said, R. Candid, F. S. R. Juan, M. T. M. Carmen and M. S. Vicente, *Cryst. Growth Des.*, 2011, **11**, 3790.

24 T. T. John, M. Mathew, K. C. Sudha, K. P. Vijayakumar, T. Abe and Y. Kashiwaba, *Sol. Energy Mater. Sol. Cells*, 2005, **89**, 27.

25 T. Dedova, O. Volobujeva, J. Klauson, A. Mere and M. Krunks, *Nanoscale Res. Lett.*, 2007, **2**, 391.

26 D. Briggs and M. P. Seah, in *Practical Surface Analysis: Auger and X-ray Photoelectron Spectroscopy*, ed. D. Briggs and M. P. Seah, John Wiley and Sons, Chichester, UK, 2nd edn, 1990, vol. **1**, p. 156.

27 M. M. Haridas and J. R. Ballare, *Colloids Surf., A*, 1998, **133**, 165.

28 J. Liang, H. Z. Wu, Y. F. Lao, N. B. Chen, P. Yu and T. N. Xu, *Appl. Surf. Sci.*, 2005, **252**, 1147.

29 M. D. Gustavo and R. C. James, *Phys. Rev. Lett.*, 2006, **96**, 226802.

30 C. E. Steven, Z. Lijun, I. H. Michael, L. E. Alexander, A. K. Thomas and J. Norris, *Nature*, 2005, **436**, 91.

31 S. Detlev, B. Rainer, K. Detlef, S. Tobias and T. Elvira, *J. Cryst. Growth*, 2011, **33**, 118.

32 B. D. Cullity and S. R. Stock, *Elements of X-rays Diffraction*, Prentice Hall, New Jersey, USA, 3rd edn, 2001, p. 619.

33 A. Ohtomo, M. Kawasaki, T. Koida, K. Masubuchi, H. Koinuma, Y. Sakurai, Y. Yoshida, T. Yasuda and Y. Segawa, *Appl. Phys. Lett.*, 1998, **72**, 2466.

34 C. Y. Liu, H. Y. Xu, L. Wang, X. H. Li and Y. C. Liu, *J. Appl. Phys.*, 2009, **106**, 073518.

35 D. Sameer, P. Swanand, V. N. T. K. Satyanarayana and S. Sudipta, *Appl. Phys. Lett.*, 2005, **87**, 133113.

36 G.-H. Ning, X.-P. Zhao and J. Li, *Opt. Mater.*, 2004, **27**, 1.